2011

Characterization of Three-Dimensional Spatial Aggregation and Association Patterns of Brown Rot Symptoms within Intensively Mapped Sour Cherry Trees

Sydney E. Everhart
University of Georgia, Athens, everhart@unl.edu

Ashley Askew
University of Georgia, Athens, aaskew@uga.edu

Lynne Seymour
University of Georgia, Athens

Imre J. Holb
University of Debrecen

Harald Scherm
University of Georgia, Athens, scherm@uga.edu

Published in *Annals of Botany* 108 (2011), pp. 1195–1202; doi:10.1093/aob/mcr029

Submitted October 29, 2010; revised December 2, 2010; accepted January 7, 2011; published electronically February 17, 2011.

Characterization of Three-Dimensional Spatial Aggregation and Association Patterns of Brown Rot Symptoms within Intensively Mapped Sour Cherry Trees

Sydney E. Everhart,[1] Ashley Askew,[2] Lynne Seymour,[2] Imre J. Holb,[3,4] and Harald Scherm[1]

1. Department of Plant Pathology, University of Georgia, Athens, GA 30602, USA
2. Department of Statistics, University of Georgia, Athens, GA 30602, USA
3. Center for Agricultural Sciences, University of Debrecen, H-4015 Debrecen, Hungary
4. Plant Protection Institute, Hungarian Academy of Sciences, H-1525 Budapest, Hungary

Corresponding author – Harald Scherm, email scherm@uga.edu

Abstract

Background and Aims – Characterization of spatial patterns of plant disease can provide insights into important epidemiological processes such as sources of inoculum, mechanisms of dissemination, and reproductive strategies of the pathogen population. While two-dimensional patterns of disease (among plants within fields) have been studied extensively, there is limited information on three-dimensional patterns within individual plant canopies. Reported here are the detailed mapping of different symptom types of brown rot (caused by *Monilinia laxa*) in individual sour cherry tree (*Prunus cerasus*) canopies, and the application of spatial statistics to the resulting data points to determine patterns of symptom aggregation and association. *Methods* – A magnetic digitizer was utilized to create detailed three-dimensional maps of three symptom types (blossom blight, shoot blight, and twig canker) in eight sour cherry tree canopies during the green fruit stage of development. The resulting point patterns were analyzed for aggregation (within a given symptom type)

and pairwise association (between symptom types) using a three-dimensional extension of nearest-neighbor analysis. *Key Results* – Symptoms of *M. laxa* infection were generally aggregated within the canopy volume, but there was no consistent pattern for one symptom type to be more or less aggregated than the other. Analysis of spatial association among symptom types indicated that previous year's twig cankers may play an important role in influencing the spatial pattern of current year's symptoms. This observation provides quantitative support for the epidemiological role of twig cankers as sources of primary inoculum within the tree. *Conclusions* – Presented here is a new approach to quantify spatial patterns of plant disease in complex fruit tree canopies using point pattern analysis. This work provides a framework for quantitative analysis of three-dimensional spatial patterns within the finite tree canopy, applicable to many fields of research.

Keywords: spatial statistics, point pattern analysis, canopy architecture, *Monilinia*, brown rot, *Prunus*, magnetic digitizer, 3-D

Introduction

Characterization of spatial patterns and spatial dynamics of plant disease can provide insights into important epidemiological processes, especially those related to sources of inoculum, mechanisms of propagule dissemination, and reproductive strategies of the pathogen population (Wu and Subbarao, 2004). For brown rot disease of pome and stone fruits, caused by fungi within the genus *Monilinia*, temporal epidemiological aspects of disease development have been well characterized (Byrde and Willetts, 1977), but information about spatial aspects of brown rot epidemics is currently limited. The temporal sequence of disease progression includes pathogen survival either on fruit mummies on the ground, on mummies in the tree, or in twig cankers, followed by primary infection of flowers (causing blossom blight) in the spring. These infections can be initiated by sexual ascospores or asexual conidia. Blossom infections can subsequently lead to shoot blight, whereby the distal portion of the shoot is killed back due to girdling at the point of infection (i.e., the development of a twig canker). Conidia produced on blighted blossoms or in twig cankers can be wind or rain-splash dispersed (Corbin et al., 1968; Pauvert et al., 1969) to infect injured green fruit in the tree or thinned fruit on the ground, providing a bridge for subsequent infection of mature fruit near harvest. This then leads to the formation of fruit mummies and/or twig cankers, providing overwintering sites for the pathogen (Landgraf and Zehr, 1982; Biggs and Northover, 1985, 1988a, b; Hong et al., 1999; Luo and Michailides, 2001; Holb and Scherm, 2007).

Spatial epidemiological aspects of brown rot development in fruit orchards have received considerably less attention than the aforementioned temporal dynamics. Two-dimensional spatial patterns, such as aggregation of symptomatic trees at the orchard scale, have been investigated by van Leeuwen et al. (2000) and Xu et al. (2001) in pome fruits. In general, these studies showed that infected trees were spatially clustered within orchard rows, with variable intensity of disease among individual trees. Although spatial patterns were more pronounced in pear (*Pyrus communis*) than in apple (*Malus domestica*) orchards, wounding of the fruit by birds, insect damage, or growth cracks was considered an influential source of the spatial pattern in both species. In a separate study, Elmer et al. (1998) examined the two-dimensional spatial pattern of *Monilinia fructicola* strains resistant

to dicarboximide fungicide in peach and nectarine (*Prunus persica*) orchards, reporting that resistant strains were mostly restricted to individual trees with no spatio-temporal correlations from year to year of trees harboring resistant strains. This suggested that resistant strains may be reestablished annually from external sources rather than overwintering and establishing from within the same tree. Although providing useful epidemiological information, such spatial analyses have not yet been extended to three dimensions to include patterns at the canopy level. Given the complex structure of tree canopies (Costes et al., 2006) adding a third dimension could reveal considerable additional detail about spatial structure, specifically with regard to disease symptom aggregation as well as associations among different symptom types within the canopy.

In general, the number of studies of three-dimensional (3-D) patterns within tree canopies is limited, largely due to the complexity of such canopies and the difficulty in developing methods to rapidly and accurately map the hundreds or thousands of points that make up the tree canopy. Where plant disease or pest injury within a tree canopy has been examined, studies have generally relied on dividing and monitoring disease or injury within investigator-specified quadrats or sectors of the canopy, such as upper, middle, and lower sections (Andrews et al., 1980; Lewis, 1992; Michailides and Morgan, 1998; Spósito et al., 2008). In addition, extending commonly used spatial statistics from two to three dimensions is not trivial mathematically. Scheuerell (2004) and Widder and Johnsen (2000) have published distance-based methods for analyzing patterns in the aggregation and association of species in three dimensions and for testing for departure from randomness.

In the present study, a magnetic digitizer was used to map different brown rot symptom types (blossom blight, shoot blight, and twig cankers) in individual sour cherry (*Prunus cerasus*) tree canopies, and 3-D methods of spatial statistics applied to the resultant data points. The goal was to determine the level of aggregation of different symptom types in the canopy as well as the degree of association of current year's symptoms with symptoms that resulted from the previous year's infections.

Materials and Methods

Mapping symptomatic elements within tree canopies

The study was conducted in an organically managed sour cherry orchard near Eperjeske, Hungary (47°31′60″N, 21°37′60″E), in June 2008 during the green fruit stage of development. Trees of cultivar Újfehértói fürtös, grafted on *P. mahaleb* rootstock, were approximately 11 years old (planted in 1997), between 2.3 and 3.8 m tall, and spaced 4.0 and 6.0 m within and between rows, respectively. At the time of the assessment, three main symptom types (blossom blight, shoot blight, and twig canker) caused by *Monilinia laxa* were present and readily distinguishable.

Eight trees (table 1) of different sizes and with varying levels of disease incidence were selected for digitizing with a FASTRAK 3Space magnetic digitizer (Polhemus, Colchester, Vermont, USA) (Smith and Curtis, 1996). The x, y, and z coordinates of all symptomatic elements were digitized using a stylus attached to the FASTRAK 3Space system, as were all asymptomatic (healthy) fruit for a total of up to 1811 data points per tree (table 1 and fig. 1). In addition, the age of each symptom (i.e., current vs. previous year) was noted,

based on whether it occurred on current or previous year's twig growth. Each digitized canopy element was tagged with colored tape to ensure that points were not measured twice and that no relevant point was omitted. The base of the trunk was designated as the origin of the coordinate system for each tree (fig. 1).

Table 1. Summary of point patterns of brown rot symptoms (caused by *Monilinia laxa*) in the canopies of eight sour cherry trees mapped in three dimensions with a magnetic digitizer

			Symptomatic elements			Specific symptom types*		
Tree no.	Total points	Asympto-matic fruit	Previous year	Current year	Total	Blossom blight	Shoot blight	Twig canker
I	261	170	35	56	91	64	19	23
II	268	146	59	63	122	71	19	43
III	643	499	54	90	144	105	43	24
IV	358	137	100	121	221	160	31	60
V	397	81	135	181	316	245	32	75
VI	1335	985	128	222	350	245	53	4
VII	1108	526	235	347	582	439	80	134
VIII	1811	1004	319	488	807	543	92	235
Mean	773	444	133	196	329	234	46	85

* Each symptomatic element may display more than one symptom type, hence the sum of the three specific symptom types is usually greater than the total number of symptomatic elements.

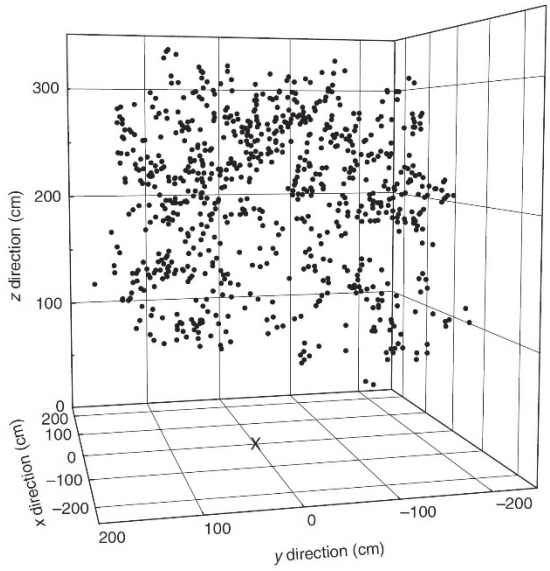

Figure 1. Positions of all 807 brown rot symptoms (blossom blight, blighted shoots, and twig cankers) as mapped in the field in three dimensions with a magnetic digitizer in the canopy of sour cherry tree no. VIII. The data point at the origin (0,0,0) marks the base of the trunk.

Spatial pattern analysis

Spatial patterns of aggregation for a given symptom type within the canopy were characterized based on nearest-neighbor distances, i.e., the shortest Euclidian distance between symptoms derived from the x, y, and z coordinates of points. The frequency distribution of nearest-neighbor distances within each tree could then be used to determine deviation from randomness (Coomes et al., 1999; Scheuerell, 2004). Aggregation was assessed using two different frames of reference: (1) deviation of all symptomatic elements from complete spatial randomness (CSR) within the canopy; and (2) deviation of a given symptom type from the baseline distribution of all symptomatic elements within each tree. In the former case (deviation from CSR), first a minimum canopy volume for each tree was simulated using the following procedure. A large volume comprising individual 0.125-m^3 cubes (50 × 50 × 50 cm) was formulated that contained all points digitized from the tree being modeled. To improve the fit of the volume to the canopy, the algorithm checked each of the cubes on the outermost layer for presence or absence of observations (points). For a given cube, if no observations were found, then it was removed from the volume. This procedure was applied until no cubes without observations were left on the exterior of the canopy volume. This resulted in a complex canopy consisting of 90–360 individual 0.125-m^3 cubes per tree, had no interior gaps, and mimicked the observed tree canopy better than a spherical or ellipsoidal canopy approximation. In the next step, 1000 Monte-Carlo simulations with random placement of all symptomatic elements were conducted within the simulated canopy volume. The cumulative frequency distribution of the actual nearest-neighbor distances between symptoms was compared with that of the Monte-Carlo simulations using a Kolmogorov-Smirnov test. If symptoms were more aggregated than when assigned randomly within the canopy, the cumulative frequency distribution would be above the upper 95% confidence band for the CSR simulations, whereas if data were regular it would fall below the lower confidence band. The test statistic d_w, the maximum departure of the observed cumulative frequency distribution from that obtained for the simulations, was calculated as described in Coomes et al. (1999) and was used as an index of aggregation; a positive value of d_w indicates aggregation, whereas a negative value signifies uniformity.

To assess deviation of a given symptom type from the distribution of all symptomatic elements within each tree, the measured coordinates of all symptomatic elements served as an empty set of points (baseline) over which the symptom of interest (such as blossom blight or twig canker) was assigned randomly without replacement to generate each of the 1000 Monte-Carlo simulations for each tree. Cumulative frequency distributions of nearest-neighbor distances and the resultant d_w values were used to assess the magnitude and significance of deviation from randomness.

Nearest-neighbor distances were also used to quantify the degree of pairwise association between different symptom types within the canopy. Here, nearest-neighbor distances were defined as the shortest distance from a given symptom of type A (e.g., blossom blight) to that of type B (e.g., twig canker). Again, the measured coordinates of all symptomatic elements served as a set of points over which the two symptom types of interest were randomized 1000 times. In each iteration, no symptoms of the same type were allowed to occupy the same coordinates, and co-occurrence of different symptom types at the same coordinate was limited to the same number observed in the actual dataset. The cumulative

frequency distribution of the actual nearest-neighbor distances between the two symptom types was compared with that of the Monte-Carlo simulations as described for the aggregation analyses above. All computations were carried out in MATLAB v. 7.10 (MathWorks, Natick, Massachusetts, USA).

Results

On average, each of the eight digitized trees contained 773 data points, of which 444 and 329 were asymptomatic fruit and symptomatic elements, respectively (table 1). More than half of the symptomatic elements were due to current year's infections (mostly blossom blight), with the remainder being remnants of previous year's infections (primarily twig cankers). Overall, about two-thirds of the specific symptoms were due to blossom blight, with twig cankers and especially shoot blight being less common. Nearest-neighbor distances computed across the eight digitized trees showed that current year's infections were closest to previous year's twig cankers (median 20.6 cm) and blighted blossoms (34.9 cm), whereas greater distances were found to previous year's shoot blight symptoms (70.4 cm) (fig. 2). These distances were inversely proportional to the number of symptoms in each symptom type class.

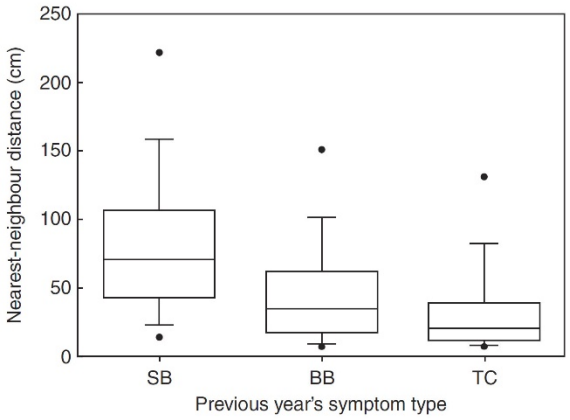

Figure 2. Nearest-neighbor distances between all current year's brown rot symptoms and previous year's shoot blight (SB), blossom blight (BB), and twig cankers (TC) in the canopies of eight sour cherry trees mapped in the field in three dimensions with a magnetic digitizer.

Results of the spatial analysis of symptomatic elements are illustrated in figure 3 for tree no. VIII, the largest tree in the dataset (1811 total points). The most common nearest-neighbor distance among the 807 *M. laxa*-associated symptoms in this tree was 7–9 cm, which was considerably shorter than the most common nearest-neighbor distance (18–24 cm) obtained by Monte-Carlo simulation within the entire tree volume (fig. 3A), suggesting aggregation relative to CSR. This was confirmed by comparative analysis of the cumulative frequency distributions of observed and simulated nearest-neighbor distances, yielding a

significant ($P < 0.001$) d_w value of 0.584 (fig. 3B). This value can be interpreted to mean that 58.4% more of the actual symptoms were spaced at a distance equal to or less than approximately 15 cm from each other, as compared with the random simulation. When similar calculations were conducted for the remaining seven trees, symptomatic elements were found to be significantly aggregated compared with CSR in each case, with d_w ranging from 0.522 to 0.657 (table 2). Thus, nearest-neighbor distances for symptomatic elements were significantly shorter than expected if they were distributed randomly within the canopy.

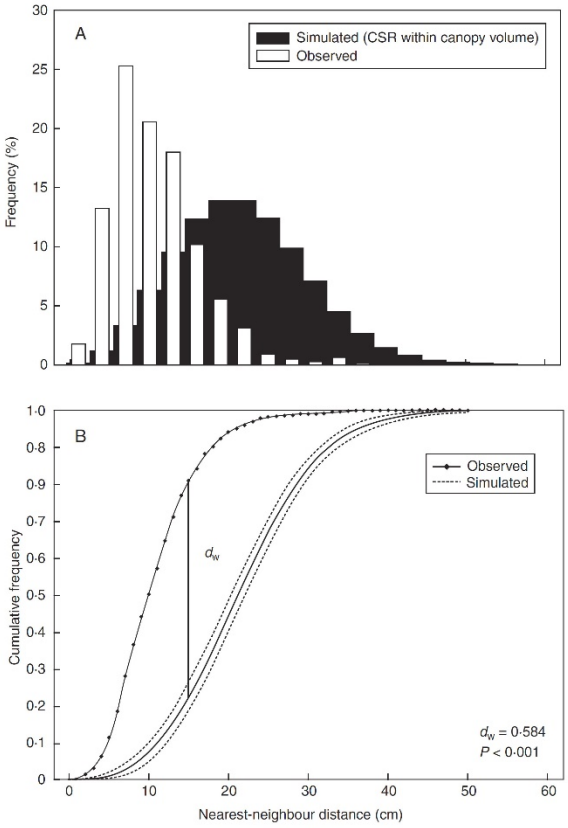

Figure 3. Frequency histogram (A) and cumulative frequency distribution (B) of observed nearest-neighbor distances of all brown rot symptoms in the canopy of sour cherry tree no. VIII, as compared with a simulation assuming complete spatial randomness (CSR) within the canopy volume. The index d_w denotes the maximum deviation between the observed and the randomly simulated cumulative frequency distributions, as indicated; in this case, a significant positive d_w value indicates aggregation of symptoms compared with CSR. The dotted lines indicate the upper and lower 95% confidence bands around the simulation.

Table 2. Index of aggregation (d_w) along with corresponding P-values (in parenthesis) for point patterns of brown rot symptoms (caused by *Monilinia laxa*) in the canopies of eight sour cherry trees mapped in three dimensions with a magnetic digitizer*

	Tree number†							
Symptom type	I (n = 91)	II (n = 122)	III (n = 145)	IV (n = 221)	V (n = 313)	VI (n = 330)	VII (n = 582)	VIII (n = 807)
Compared with complete spatial randomness within canopy volume								
All symptoms	**0.522 (<0.001)**	**0.607 (<0.001)**	**0.588 (<0.001)**	**0.634 (<0.001)**	**0.523 (<0.001)**	**0.657 (<0.001)**	**0.623 (<0.001)**	**0.584 (<0.001)**
Compared with observed distribution of all symptomatic elements								
Current year's symptoms	**–0.199 (0.007)**	**–0.231 (0.004)**	–0.106 (0.126)	–0.048 (0.051)	**–0.159 (<0.001)**	**–0.112 (<0.001)**	**–0.124 (<0.001)**	**–0.157 (<0.001)**
Previous year's symptoms	0.131 (0.657)	**–0.180 (0.041)**	**–0.229 (0.013)**	**0.473 (0.001)**	0.047 (0.901)	**–0.213 (<0.001)**	–0.034 (0.924)	**–0.156 (<0.001)**
Blossom blight	–0.114 (0.175)	–0.154 (0.056)	0.0600 (0.490)	**–0.094 (0.039)**	–0.054 (0.138)	–0.056 (0.203)	–0.046 (0.078)	**–0.121 (<0.001)**
Twig blight	–0.155 (0.712)	–0.169 (0.227)	0.206 (0.376)	–0.130 (0.371)	–0.150 (0.140)	**–0.295 (<0.001)**	–0.116 (0.093)	**–0.168 (<0.001)**
Shoot blight	–0.179 (0.713)	0.129 (0.934)	0.225 (0.111)	0.339 (0.016)	–0.925 (0.0951)	0.145 (0.349)	0.148 (0.189)	0.070 (0.885)

* d_w values calculated based on the cumulative frequency distribution of nearest-neighbor distances between symptoms of the same type. Significant positive values ($P \leq 0.05$; in bold) indicate aggregation, whereas significant negative values correspond to a more regular distribution compared with the random simulation.

† Trees arranged in order of increasing size (number of symptoms).

The next step of the analysis evaluated the deviation of each specific symptom type from the baseline distribution of all symptomatic elements within a given tree. In the majority of symptom type–tree combinations (24 out of 40), no significant deviation from the baseline distribution was observed (table 2). In most of the cases where d_w was statistically significant (14 out of 16), symptoms were less aggregated (i.e., more uniform) than the baseline of all symptomatic elements. An illustrative example of this is given in figure 4 for blossom blight in tree no. VIII. Only two symptom type–tree combinations (previous year's symptoms and shoot blight in tree no. IV) showed significant aggregation compared with the baseline (table 2). Thus, whereas *M. laxa*-associated symptoms were generally aggregated within the overall canopy volume (based on the above comparison with CSR), there was little evidence that specific symptom types were more or less aggregated than the overall pattern of all symptomatic elements within the tree.

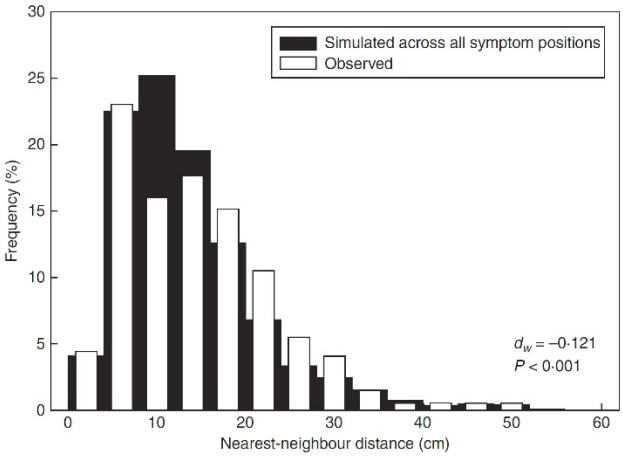

Figure 4. Frequency histogram of nearest-neighbor distances between blighted blossoms in the canopy of sour cherry tree no. VIII, as compared with a simulation assigning the blossom blight symptoms randomly across the coordinates of all symptomatic elements within the tree. The index d_w denotes the maximum deviation between the observed and the randomly simulated cumulative frequency distributions; in this case, a significant negative d_w value indicates a more regular distribution of blossom blight compared with all brown rot symptoms in the tree.

Pairwise association analyses showed that all trees, with the exception of tree no. I (the smallest tree), had significant associations (either positive or negative) between one or more symptom types, with the most common significant d_w values found when testing association of all current year's symptoms with all previous year's symptoms (table 3). In this case, only tree no. IV showed a negative association, whereas all others were positive, indicating that nearest-neighbor distances between these two symptom types were generally shorter than expected by chance alone. This is illustrated in figure 5, again using tree no. VIII as an example. Five trees each showed significant associations between all current year's symptoms and previous year's twig cankers and between current year's blossom blight and previous year's twig cankers. In contrast, only two associations between blossom blight and twig cankers (regardless of age) were statistically significant. Whether a significant association was positive or negative appeared to depend more on the tree than on the symptom type examined (table 3).

Table 3. Index of association (d_w) along with corresponding *P*-values (in parenthesis) for point patterns of brown rot symptoms (caused by *Monilinia laxa*) in the canopies of eight sour cherry trees mapped in three dimensions with a magnetic digitizer*

	Tree number†							
Symptom type	I (n = 91)	II (n = 122)	III (n = 145)	IV (n = 221)	V (n = 313)	VI (n = 330)	VII (n = 582)	VIII (n = 807)
Current year's to previous year's symptoms								
	0.1488	**0.1943**	**0.1922**	**–0.2925**	**0.1005**	**0.1860**	**0.0957**	**0.1791**
	(0.112)	**(0.008)**	**(0.009)**	**(<0.001)**	**(0.025)**	**(<0.001)**	**(0.003)**	**(<0.001)**
Current year's symptoms to previous year's twig cankers								
	0.0842	**0.1862**	0.1317	**–0.2103**	**–0.1411**	**0.1024**	0.0736	**0.1615**
	(0.664)	**(0.018)**	(0.156)	**(<0.001)**	**(0.005)**	**(0.038)**	(0.061)	**(<0.001)**
Blossom blight to twig cankers								
	0.0451	0.1458	–0.0792	–0.0767	**–0.1388**	0.0480	0.0587	**0.1034**
	(0.968)	(0.079)	(0.484)	(0.220)	**(0.003)**	(0.558)	(0.110)	**(<0.001)**
Current year's blossom blight to previous year's twig cankers								
	0.1130	**0.2092**	0.1120	**–0.2421**	**–0.1152**	**0.1223**	0.0660	**0.1624**
	(0.366)	**(0.004)**	(0.214)	**(<0.001)**	**(0.026)**	**(0.006)**	(0.112)	**(<0.001)**

* d_w values calculated based on the cumulative frequency distribution of nearest-neighbor distances between symptoms of different types. Significant positive values ($P \leq 0.05$; in bold) indicate that the observed symptoms of the two types are closer together than in the random simulation, whereas significant negative values correspond to a more regular distribution of the two symptom types to each other. For the random simulation, the measured coordinates of all symptomatic elements within each tree served as an empty set of coordinates over which the two symptom types of interest were randomized.

† Trees arranged in order of increasing size (number of symptoms).

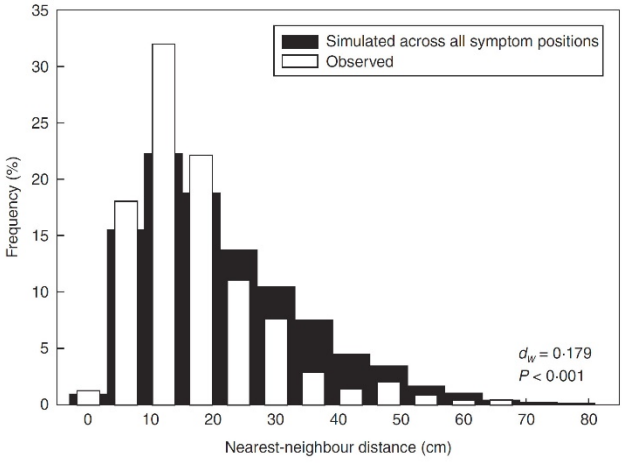

Figure 5. Frequency histogram of nearest-neighbor distances between all current year's brown rot symptoms and previous year's twig cankers in the canopy of sour cherry tree no. VIII, as compared with a simulation assigning the two symptom types randomly across the coordinates of all symptomatic elements within the tree. The index d_w denotes the maximum deviation between the observed and the randomly simulated cumulative

frequency distributions; in this case, a significant positive d_w value indicates association, i.e., the observed symptoms of the two types are closer together than in the random simulation.

Discussion

Presented here is the first study to quantify spatial patterns of plant disease in complex three-dimensional fruit tree canopies using nearest-neighbor analysis. Although previous workers have collected data on disease and pest injury within individual trees, the spatial resolution used in earlier studies was generally lower (e.g., as a result of using a limited number of strata or quadrats within the canopy to summarize patterns) and/or the statistical analyses were more limited in scope (e.g., comparisons between the upper vs. lower or exterior vs. interior canopy). For example, dividing the canopy of fig trees (*Ficus carica* "Calimyrna") into high or low, north or south, and inner or outer layers, the spread of a fungal pathogen via fig-pollinating wasps showed no significant difference in disease incidence based on an analysis of variance (Michailides and Morgan, 1998). Similarly, the canopy of coast live oak trees (*Quercus agrifolia*) was divided into nine sectors, corresponding to upper, middle, and lower portions combined with northeast, south, and northwest cardinal directions, in order to examine the distribution of weevil-infested acorns (Lewis, 1992). The statistical analysis (analysis of variance and pairwise comparison) of the 36 trees, each assessed for one of the nine canopy quadrats, showed three of the nine quadrats to have significantly more larval infestation than the others. Compared with these quadrat-based studies, the combination of rapid point pattern collection with a high-precision magnetic digitizer (Moulia and Sinoquet 1993; Smith and Curtis, 1996) and data analysis using a 3-D extension of nearest-neighbor statistics (Scheuerell, 2004) has made it possible to quantify aggregation and association patterns for different symptom types within the canopy both efficiently and effectively.

This pilot study showed that symptoms associated with *M. laxa* infection in sour cherry trees are generally aggregated within the canopy volume, but that there is no consistent pattern for one symptom type to be more or less aggregated than the other (table 2). This result could have been related to the high disease pressure in this organically managed orchard, which may have masked differences in disease aggregation patterns among symptom types that may be more apparent in conditions of lower disease incidence. Alternatively, a pronounced effect of environmental heterogeneity within the canopy (e.g., differences in localized moisture availability) could have resulted in similar patterns of disease aggregation across symptom types. Heterogeneity in surface wetness, a prerequisite for infection by most fungal plant pathogens, can be marked in fruit tree canopies (Sentelhas et al., 2005) and can significantly impact disease development (Batzer et al., 2008).

Interestingly, results of the pairwise association analyses showed that current year's symptoms were generally (in six out of eight trees evaluated) closer to previous year's symptoms than expected by chance alone (table 3), providing statistical support for the long-standing notion (based on disease cycle research with *Monilinia* spp.) that proximity to within-tree inoculum sources is important for disease progression from one year to the

next (Landgraf and Zehr, 1982; Biggs and Northover, 1985, 1988a, b; Hong et al., 1999; Luo and Michailides, 2001; Holb and Scherm, 2007). For spores that are primarily airborne, such as those of *Monilinia* spp. (Corbin et al., 1968), the presence of a pronounced dispersal gradient would readily explain the observed association between current and previous year's symptoms. Rain-splashing (Pauvert et al., 1969) and run-off transport of spores in rain water from twig inoculum sources to other susceptible canopy elements would also favor the short-distance association between current and previous year's symptoms, as has been documented for *Venturia carpophila*, another twig-borne pathogen in peach canopies (Lan and Scherm, 2003).

Although associations of current year's symptoms with specific symptom types from the previous year were not consistently significant (possibly because of smaller sample sizes), it is reasonable to assume that twig cankers formed in the previous year would serve as the most important within-tree inoculum source because of their relatively large number and, consequently, their shorter average distance to current year's symptoms (fig. 2). Stensvand et al. (2001) previously documented that sporulation of *M. laxa* on twig cankers of sweet cherry (*Prunus avium*) peaks around the time of bloom, further supporting the role of twig cankers as a key inoculum source for inciting blossom blight (the most frequent current season's symptom in the present study).

Since the organically managed orchard used for this study had very high brown rot levels, it would be important to confirm the aggregation and association patterns observed here in conditions of lower disease pressure, e.g., in orchards managed using conventional or integrated practices. Spatial patterns are likely to be dependent on the overall levels of disease in a tree, as suggested by the variations in aggregation and association patterns across the eight trees included in the present study (tables 2 and 3).

Overall, the results of these analyses quantitatively confirm the role of different symptom types in shaping the pattern of brown rot development within the tree canopy. More importantly, the methodologies for data collection and analysis described here have broader applicability, potentially allowing their use in a range of canopy ecology studies. We are currently working to extend the approach to second-order analyses (considering more than just the nearest neighbor of each point in the analysis of aggregation and association), and also to include a temporal element by digitizing symptomatic elements over time as the epidemic develops. We are further collecting pathogen isolates from all infected elements within each tree to determine the fine-scale genetic structure (Trapnell et al., 2004) of the pathogen population at the canopy level. We hope that these analyses will help to develop a deeper understanding of patterns of pathogen survival, spread, and reproductive strategies within tree canopies.

Acknowledgments – This study was supported by the Hungarian Scientific Research Fund (grant no. HSRF 78339), a János Bolyai Research Fellowship and the Southern-Region IPM Program (grant no. 2009-34103-19818).

Literature Cited

Andrews JH, Kenerley CM, Nordheim EV. 1980. Positional variation in phylloplane microbial populations within an apple tree canopy. *Microbial Ecology* 6: 71–84.

Batzer JC, Gleason ML, Taylor SE, Koehler KJ, Monteiro JEBA. 2008. Spatial heterogeneity of leaf wetness duration in apple trees and its influence on performance of a warning system for sooty blotch and flyspeck. *Plant Disease* 92: 164–170.

Biggs AR, Northover J. 1985. Inoculum sources for *Monilinia fructicola* in Ontario peach orchards. *Canadian Journal of Plant Pathology* 7: 302–307.

Biggs AR, Northover J. 1988a. Early and late-season susceptibility of peach fruits to *Monilinia fructicola*. *Plant Disease* 72: 1070–1074.

Biggs AR, Northover J. 1988b. Influence of temperature and wetness duration on infection of peach and sweet cherry fruits by *Monilinia fructicola*. *Phytopathology* 78: 1352–1356.

Byrde RJW, Willetts HJ. 1977. *The brown rot fungi of fruit: their biology and control*. Oxford: Pergamon.

Coomes DA, Rees M, Turnbull L. 1999. Identifying aggregation and association in fully mapped spatial data. *Ecology* 80: 554–565.

Corbin JB, Ogawa JM, Schultz HB. 1968. Fluctuations in numbers of *Monilinia laxa* conidia in an apricot orchard during the 1966 season. *Phytopathology* 58: 1387–1394.

Costes E, Lauri PÉ, Regnard JL. 2006. Analyzing fruit tree architecture: implications for tree management and fruit production. *Horticultural Reviews* 32: 1–61.

Elmer PAG, Gaunt RE, Frampton CM. 1998. Spatial and temporal characteristics of dicarboximide-resistant strains of *Monilinia fructicola* and brown rot incidence in stone fruit. *Plant Pathology* 47: 530–536.

Holb IJ, Scherm H. 2007. Temporal dynamics of brown rot in different apple management systems and importance of dropped fruit for disease development. *Phytopathology* 97: 1104–1111.

Hong C, Holtz BA, Morgan DP, Michailides TJ. 1999. Significance of thinned fruit as source of the secondary inoculum of *Monilinia fructicola* in California nectarine orchards. *Plant Disease* 81: 519–524.

Lan Z, Scherm H. 2003. Moisture sources in relation to conidial dissemination and infection by *Cladosporium carpophilum* within peach canopies. *Phytopathology* 93: 1581–1586.

Landgraf FA, Zehr E. 1982. Inoculum sources for *Monilinia fructicola* in South Carolina peach orchards. *Phytopathology* 72: 185–190.

van Leeuwen GCM, Stein A, Holb I, Jeger MJ. 2000. Yield loss in apple caused by *Monilinia fructigena* (Aderh. & Ruhl.) Honey, and spatiotemporal dynamics of disease development. *European Journal of Plant Pathology* 106: 519–528.

Lewis VR. 1992. Within-tree distribution of acorns infested by *Curculio occidentalis* (Coleoptera: Curculionidae) and *Cydia latiferreana* (Lepidoptera: Tortricidae) on coast live oak. *Environmental Entomology* 25: 975–982.

Luo Y, Michailides TJ. 2001. Risk analysis for latent infection of prune by *Monilinia fructicola* in California. *Phytopathology* 91: 1197–1208.

Michailides TJ, Morgan DP. 1998. Spread of endosepsis in calimyrna fig orchards. *Phytopathology* 88: 637–647.

Moulia B, Sinoquet H. 1993. Three-dimensional digitizing systems for plant canopy geometrical structure: a review. In: Varlet-Grancher C, Bonhomme R, Sinoquet H, eds. *Crop structure and light microclimate: characterization and applications*. Paris: INRA, 183–193.

Pauvert P, Fournet J, Rapilly F. 1969. Etudes sur la dispersion d'un inoculum par des gouttes d'eau en fonction du conceptacle sporifère. *Annales de phytopathologie* 1: 491–493.

Scheuerell MD. 2004. Quantifying aggregation and association in three-dimensional landscapes. *Ecology* 85: 2332–3240.

Sentelhas PC, Gillespie TJ, Batzer JC, et al. 2005. Spatial variability of leaf wetness duration in different crop canopies. *International Journal of Biometeorology* 49: 363–370.

Smith GS, Curtis JP. 1996. A fast and effective method of measuring tree structure in 3 dimensions. *Acta Horticulturae* 416: 15–20.

Spósito MB, Amorim L, Bassanezi RB, Bergamin Filho A, Hau B. 2008. Spatial pattern of black spot incidence within citrus trees related to disease severity and pathogen dispersal. *Plant Pathology* 57: 103–108.

Stensvand A, Talgo V, Borve J. 2001. Seasonal production of conidia of *Monilinia laxa* from mummified fruits, blighted spurs and flowers of sweet cherry. *Gartenbauwissenschaft* 66: 273–281.

Trapnell DW, Hamrick JL, Nason JD. 2004. Three-dimensional fine-scale genetic structure of the neotropical epiphytic orchid, *Laelia rubescens*. *Molecular Ecology* 13: 1111–1118.

Widder E, Johnsen S. 2000. 3D spatial point patterns of bioluminescent plankton: a map of the "minefield." *Journal of Plankton Research* 22: 409–420.

Wu BM, Subbarao KV. 2004. Analysis of spatial patterns in plant pathology. *Recent Research Developments in Plant Pathology* 3: 167–187.

Xu X-M, Robinson JD, Berrie AM, Harris DC. 2001. Spatio-temporal dynamics of brown rot (*Monilinia fructigena*) on apple and pear. *Plant Pathology* 50: 569–578.